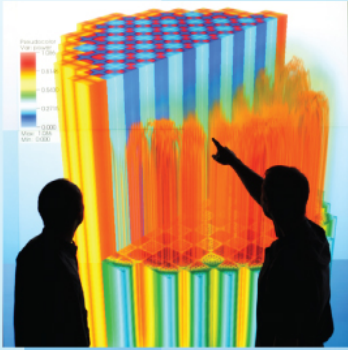


Power uprates  
and plant life extension



Engineering design  
and analysis



# Nucleation Site Density, Bubble Departure Diameter, Wait Time and Local Temperature Distribution in Subcooled Flow Boiling of Water at Atmospheric Pressure

MIT

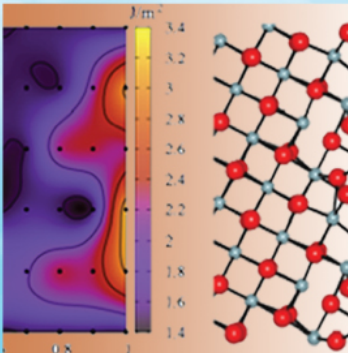
B Phillips, J Buongiorno, T McKrell

May 12-17, 2013:

Science-enabling  
high performance  
computing



Fundamental science



Plant operational data



U.S. DEPARTMENT OF  
**ENERGY**

**Nuclear Energy**

## NUCLEATION SITE DENSITY, BUBBLE DEPARTURE DIAMETER, WAIT TIME AND LOCAL TEMPERATURE DISTRIBUTION IN SUBCOOLED FLOW BOILING OF WATER AT ATMOSPHERIC PRESSURE

**B. Phillips, J. Buongiorno and T. McKrell**

Massachusetts Institute of Technology, Department of Nuclear Science and Engineering  
77 Massachusetts Ave. Cambridge, MA 02139, USA

[bren@mit.edu](mailto:bren@mit.edu), [jacopo@mit.edu](mailto:jacopo@mit.edu), [tmckrell@mit.edu](mailto:tmckrell@mit.edu)

### ABSTRACT

The physics of subcooled flow boiling of water were explored using high-speed video (HSV), and infrared (IR) thermography. HSV allowed measurement of the bubble departure diameter, and IR thermography allowed measurement of wall superheat (both the local distribution and the surface-averaged value), heat transfer coefficient, nucleation site density, and bubble wait time. The tests were performed at atmospheric pressure at a constant subcooling of 10°C. The mass flux values explored were 100, 250, 500, 750, 1000, and 1250 kg/m<sup>2</sup>-s. The heat flux values explored were 100, 200, 400, 600, 800, 1000, and 1200 kW/m<sup>2</sup>. As expected, the heat transfer coefficients increased with increasing mass flux in the single-phase convection and partial boiling regions, and they converged to a fully-developed boiling curve for high heat fluxes. The bubble departure diameter decreased with increasing mass flux and decreasing heat flux, in accord with Klausner's model. However the model systematically overpredicted the data. The nucleation site density increased with increasing superheat and decreasing mass flux, in accord with the model by Kocamustafaogullari and Ishii, which however does not account for the effect of subcooling. The bubble wait time increased with the ratio of local superheat to heat flux. The wait time correlation of Basu does not reproduce the data correctly, as it ignores the effects of subcooling and heater thermal diffusivity, which are expected to be important. Significant localized cooling was observed underneath bubbles sliding along the wall after departure from a nucleation site, an effect which should be considered in advanced models of subcooled flow boiling.

## 1. INTRODUCTION

Subcooled flow boiling is a complicated physical phenomenon present in many industrial heat transfer applications including conventional power plants and nuclear power reactors. It includes multiple heat transfer mechanisms (e.g. single phase convection, nucleate boiling, condensation, sliding bubbles), two phase flow and thermal non-equilibrium conditions existing between the vapor and the liquid phases, and is further complicated by the effects of the chemico-physical conditions (e.g. roughness, hydrophilicity, porosity) present on the boiling surface. Although, it has been studied for many years, it is difficult to fully understand the underlying physics because of limitations on the quantities and phenomena that can be accurately measured. A better understanding of subcooled flow boiling would allow for development of better codes and predictive methods, with consequent benefits for the aforementioned applications.

### 1.1 Objective

The objective for the proposed work is to generate a new set of high-resolution data on subcooled flow boiling characteristics, including bubble departure diameter, wait time, and temperature profiles of the boiling surface. This data may inspire the development of analytical models of subcooled flow boiling as well as be used to validate numerical models in CFD codes. The approaches used in CFD include the Eulerian-Eulerian, two-fluid, six-equation model [1], and closure relations momentum and energy equations can be provided by models such as the heat flux partitioning model of Kurul and Podowski [2] and Kolev's bubble interaction model [3], which require bubble departure diameter, wait and growth times, and nucleation site density as input.

### 1.2 Previous Work

Subcooled flow boiling has been extensively investigated. Here we limit the literature survey to those studies that have utilized techniques similar to the ones adopted in this study.

Del Valle and Kenning [4] measured surface temperature and used high speed photography in subcooled flow boiling with water to examine nucleation site density in a rectangular channel. They calculated the heat removed through various processes including microlayer evaporation, quenching of the surface after bubble departure, and convection and compared the total values to the experimental heat flux. They found that for their 84 K subcooled flow, quenching of the surface was the most important component of the heat transfer and the microlayer evaporation effect was negligible.

Basu et al. [5] measured the temperature distribution with thermocouples in a rod bundle. They developed a correlation for the onset of subcooled nucleate boiling based on the contact angle of the fluid with the surface, the local subcooling, and the axial location. Their correlation is for water and valid for contact angles from 1-85°, pressures from 1-137.5 bars, local liquid subcooling of 1.7-80°C, and velocities from 0 m/s-17 m/s. They found that the nucleation site density depended only on contact angle and wall superheat.

Situ et al. [6] conducted subcooled flow boiling experiments with water in an annular channel. They measured bubble parameters such as departure diameter, nucleation site density, departure frequency, and velocity after departure with high speed photography. Situ et al. [7] went on to develop a correlation for bubble departure frequency. Hong et. al [8] measured departure

diameters in stationary and heaving conditions and developed a model to predict departure diameter.

Euh et al. [9] examined bubble departure in an annular channel during subcooled boiling. They varied the test conditions over a test matrix of 167-346 kPa, mass fluxes of 214-1869 kg/m<sup>2</sup>/s, heat fluxes of 61-238 kW/m<sup>2</sup>, and subcooling of 7.5-23.4°C. They compared their data to the mechanistic models of Basu [10], Podowski et al. [11] and Situ et al [7]. They found that the data fit Situ's model well, and developed a modified form of the model to better represent their data.

Thorncroft et al. [12] performed high speed camera analysis of upward and downward flow boiling of slightly subcooled FC-87 in a square test section equipped with a heating strip. They measured the heater surface temperature at various axial positions using thermocouples. They found that the dynamics were vastly different for upward and downward flow. They also concluded that a major mechanism of heat removal was the "sliding" of the bubbles along the surface prior to their departure. A bubble can either slide along the surface, or immediately depart into the bulk fluid and collapse [13]. Bubble sliding has been further investigated such as by Li et al. [14] and they found that the distribution of bubble sliding velocities and sliding diameters was quite large. They also identified two regimes of bubble sliding. The first is for bubbles with a short lifetime whose diameters fluctuate rapidly during sliding from rapid vaporization and condensation. The second type has a longer lifetime and the diameter changes more slowly. The interaction of nucleation sites can also have an influence on the departure diameter [15], in pool boiling the closer two sites are together tends to lower the departure diameter.

Chen et al. [16] investigated how bubble characteristics varied for R-407C in a narrow rectangular annular horizontal channel using HSV. They found that the heat transfer coefficient increased with a smaller gap. They also proposed correlations for nucleation site density and bubble frequency.

Recently, Sugrue et al. [17] conducted a systematic experimental investigation of bubble departure diameter in subcooled flow boiling over a range of mass fluxes, heat fluxes, inclination angles, pressures and subcoolings. Their data indicate that the bubble departure diameter increases with increasing heat flux, decreasing mass flux, decreasing subcooling, and decreasing pressure. Also, the bubble departure diameter increases with decreasing orientation angle, i.e. the largest bubbles are found to detach from a downward-facing horizontal surface.

High speed infrared cameras have been used to capture 2D temperature profiles of the surface during boiling. The data collected has been used to measure bubble parameters, the effect of nanofluids on bubble parameters, nucleation site density, bubble interactions, and surface temperature during quenching [18, 19, 20, 21, 22, 23, 24]. There has been some work done with IR thermography to measure the wall temperature of a heater during flow boiling using very low frame rates that were unable to capture individual nucleation events [25].

## **2. EXPERIMENTAL FACILITY**

### **2.1 Flow Loop**

The flow loop consists of a pump, a flow meter, a preheater (used to maintain constant subcooling), a heat exchanger, an accumulator with a nitrogen gas over pressure, a fill and

drain tank, and various RTD and pressure sensors. The schematic is shown in Figure 1. For a detailed description of each component see Ref [26].

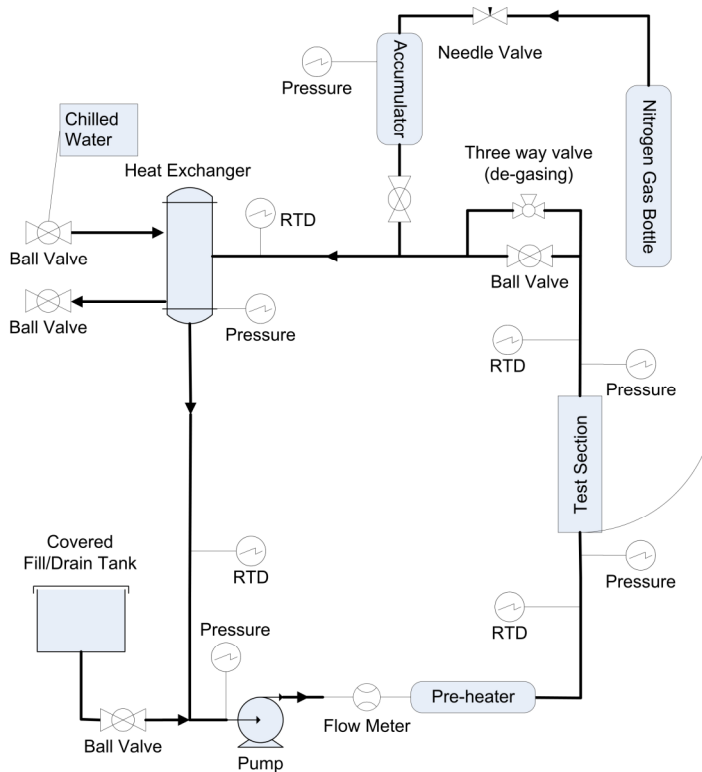


Figure 1 – Diagram of the flow loop.

## 2.2 Test Section and Heater

The test section is composed of a quartz rectangular channel with nominal dimensions of 10 mm x 30 mm and a length of 220 mm. The quartz section allows for excellent visualization from various angles for HSV images. The test section has over 6 L/D values of quartz upstream and downstream of the heater recess. On the inlet side the cell is mated with a stainless steel conduit that has the same dimensions as the quartz flow channel and is over 64 L/D long to provide for fully developed flow entering the quartz test section. The quartz section is shown in Figure 2.

The heater cartridge consists of two graphite electrodes and two Macor insulators that are epoxied and bolted together. The heater cartridge is machined to fit, and is machined to sit flush with the inside face of the channel. The small gap between the heater and the cartridge is filled with a hydrophilic sealant to minimize the nucleation sites at the interface. The gap between the heater cartridge and the flow channel is only heated by conduction, and has a small enough heat flux that nucleation does not occur at this interface. The gap is also sized such that it closes via thermal expansion when the section is at temperature. The sapphire heater is 1 mm thick with filleted edges on to ends, and is coated with an Indium-Tin Oxide (ITO), ~700 nm thick, which is the active heating element. The ITO acts as the boiling surface and has a static contact angle of 100-110°. The ITO has different surface characteristics compared to that of fuel rods, but the purpose of this work is to gain a more fundamental understanding of the various boiling parameters. The ITO transmits almost no infrared waves in the 3-5  $\mu\text{m}$  range that the IR camera is sensitive to, so the signal received by the IR camera is that of the surface and can be calibrated

to the surface temperature. The ITO wraps around the filleted edges onto the back of the sapphire where 2.5 mm silver pads are laid on top of the ITO to make the electrical connections to the heater. The sapphire heater is epoxied into the heater cartridge flush with the face of the cartridge. The active heater area is 20 mm x 10 mm with the 20 mm direction being in the direction of the flow. The channel and heater positioning is shown in Figure 2.

### 2.3 Experimental Setup

The Phantom V12.1 high speed video (HSV) camera is oriented parallel to the plane of the heater, and with its associated optics is configured to have a spatial resolution of better than 15 microns. 90 degrees from the Phantom camera, and looking at the plane of the heater is the FLIR SC6000 high speed infrared (IR) camera. The IR camera images the ITO surface, to measure the 2D temperature distribution on the surface. The IR camera is configured to have a spatial resolution of 90 microns.

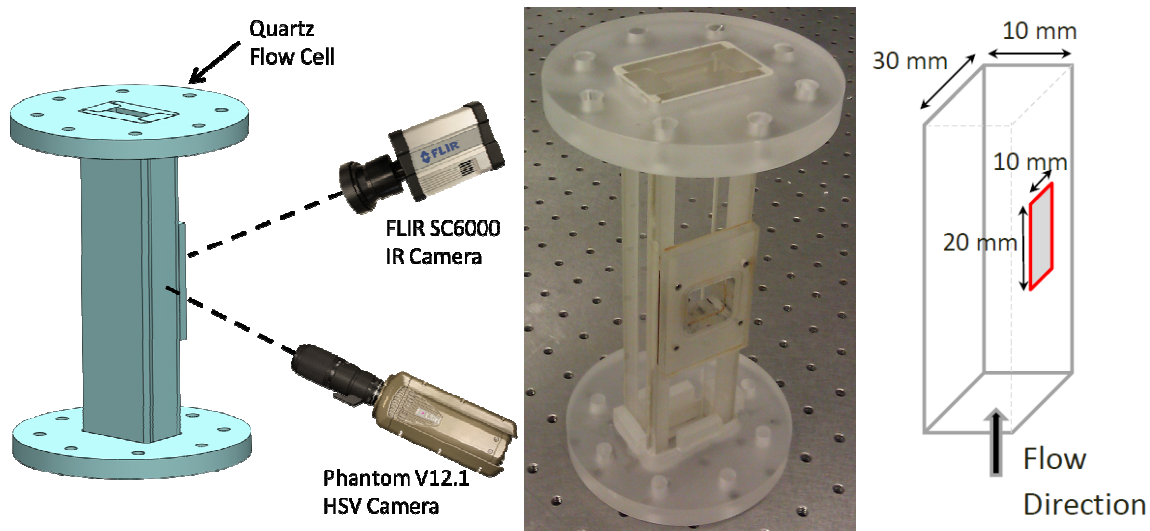


Figure 2 – Experimental setup for HSV and IR thermography (left), picture of the quartz section (middle), and diagram of flow channel with the heated area shown in red.

### 2.4 Experimental Procedure

The loop is filled with deionized water from the fill and drain tank using nitrogen gas. The pump is then started and non-condensable gasses are vented out of the system while makeup water is added through the fill tank. The preheater is started to raise the temperature of the liquid, which lowers the solubility of non-condensable gases. When the fluid reaches about 40°C the mass flux is increased to 500 kg/m<sup>2</sup>-s, and the test section heater is energized to allow for nucleate boiling to assist in degassing. When the fluid temperature reaches 60°C the temperature is stabilized by adjusting the power of the preheater and the degassing line is cycled. The degassing line valve is cycled every 10 minutes until no more bubbles emerge from the degassing line. The dissolved oxygen (DO) probe is installed and flow is aligned to the DO probe. A low reading of dissolved oxygen (5 ppm or less) confirms that the loop is degassed.

The loop bulk temperature is then set to the desired temperature for the test. The high speed video camera and the high speed IR camera are set up, and a spatial calibration is obtained for each.

When the loop temperature is stable the mass flux is adjusted to the desired level. Then the heat flux of the heater is adjusted to the desired value, and simultaneous HSV and IR images are acquired.

The temperature of the surface is determined via IR thermography. The IR camera first undergoes a non-uniformity correction using a blackbody simulator to compensate for non-uniform response in the pixels. The IR camera signal is then calibrated by imaging the heater while being heated with a thermocouple on the surface to read the average temperature. This data is used to construct a temperature vs. signal calibration curve. The average temperature on the surface is then determined using a custom MATLAB script that averages the temperature across the heater both spatially and temporally. The IR camera calibration is checked one more time in situ against the loop temperature, before the test section heater is energized. Examples of the raw IR and HSV data can be found in Figure 6 and 8.

### 3. RESULTS

The data were collected at atmospheric pressure at a constant subcooling of 10°C. The mass flux values explored were 100, 250, 500, 750, 1000, and 1250 kg/m<sup>2</sup>-s. The heat flux values explored were 100, 200, 400, 600, 800, 1000, and 1200 kW/m<sup>2</sup>.

#### 3.1 Boiling Curves and Heat Transfer Coefficients

The boiling curves and heat transfer coefficients are plotted in Figure 3.

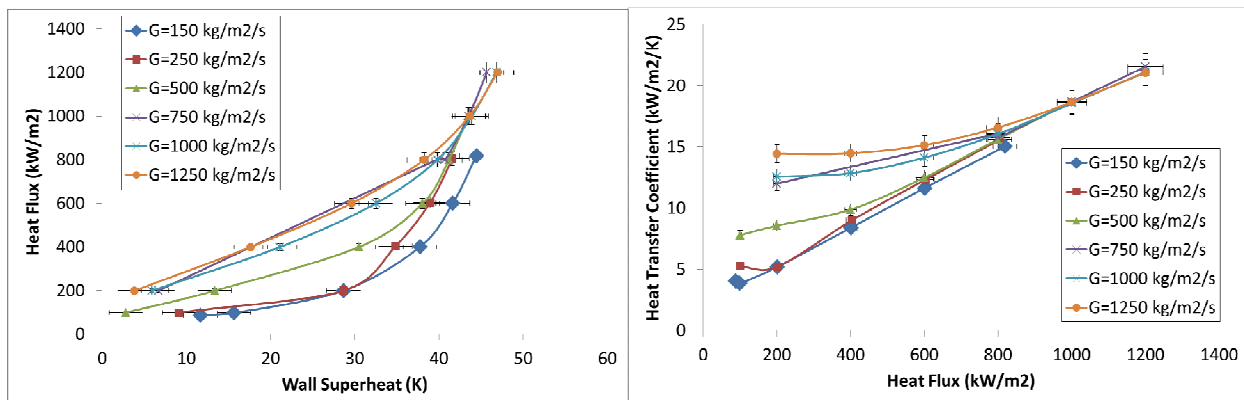


Figure 3 - Boiling curve (left) and heat transfer coefficient for 10K subcooling at 1 atmosphere. Heat flux error is 5% and wall superheat uncertainty is 2%.

The boiling curves show the classic trends of nucleate flow boiling [27]. There is a flat slope during the single phase heat transfer region. The wall superheat at the onset of nucleate boiling (ONB) increases with increasing mass flux. At ONB the boiling curve slope increases indicating a rise in the heat transfer coefficient. As the heat flux and wall superheat increase beyond ONB, nucleate boiling becomes fully-developed and the heat transfer coefficients converges to a single curve, independently insensitive to changes in mass flux.

#### 3.2 Bubble Departure Diameter, Wait Time, and Nucleation Site Density

The bubble departure diameter was measured using HSV, the spatial resolution was 15 μm per pixel and an area of 1280x800 pixels was imaged at a rate of 1000-5000 Hz, as appropriate for

the flow conditions. The bubble departure diameter is defined here as the diameter of the bubble at the time of lift-off (detachment perpendicular to the wall) or slide (detachment parallel to the wall), whichever comes first. The diameter was only measured for flow regimes in which individual bubbles could be identified and were not greatly influenced by other bubbles during their growth (i.e. no bubble coalescence on the surface). The distribution of the bubble departure diameters was much larger than the spatial resolution of the images, and the error bars on the plot in Figure 4 represent the standard deviation of the distribution. The Klausner force-balance model [28] is also shown as a comparison. This model consistently overestimates the measured departure diameter by about 75%. However, it does follow a very consistent trend with the measured data. The data shows increasing departure diameters with increasing heat flux, and decreasing departure diameters with increased mass flux as expected. These results are consistent with the observations of Sugrue et al. [17].

The wait time is defined as the time between bubble departure and nucleation of the next bubble. Effectively, it is a measure of the time required to reconstruct the thermal boundary layer following bubble departure. In this study the wait time was determined from the IR thermography images, as a bubble nucleation is marked by a sharp drop in the wall temperature, while the wall temperature starts to rise again at bubble detachment. The temporal resolution of the IR images was 1 ms. The wait time was measured by choosing individual sites near the inlet of the heater to minimize the effect of sliding bubbles on the site. The distribution of the wait time was much larger than the measurement error so the error bars represent the standard distribution of the sample. The bubble wait time data are shown in Figure 4, plotted vs. the ratio of the local nucleation superheat to the heat flux, as wait time is expected to increase with increasing nucleation temperature and decrease with increasing heat flux. However, a clear trend is not distinguishable in the data with this parameterization, likely because it does not capture the effect of mass flux on reconstruction of the thermal boundary layer. The wait times are compared to a correlation by Basu [10], which is shown in (10).

$$t_w = 139.1(\Delta T_w^{-4.1}) \quad (10)$$

The correlation is only dependent on the average wall superheat and assumes that there is no effect of subcooling, heat flux, heat transfer coefficient and heater thermal diffusivity, which are expected to be important. Not surprisingly, the correlation cannot predict the experimental values accurately. Wait times of Podowski [29] and Hsu and Graham [30] are also shown on the plot.

The nucleation site density was measured from the IR thermography images by automatically counting the sites using a custom MATLAB program. The detection algorithm takes an average value from each pixel across time and subtracts the mean value from the current frame. This highlights specific sites; a signal cutoff value is applied to leave only the nucleation sites in the image. Clusters of pixels are then identified and their centroids calculated. The site is then checked for size, if it is too large it is rejected to prevent counting nucleation sites late in the ebullition cycle. The centroids are then rounded to whole pixel values, and this coordinate is compared to previously recorded sites. A site was only counted as a new site if there was not a previous site in the nearest neighbor pixels. A convergence criterion was imposed to minimize the counting of noise as nucleation sites. For example, if an infinite number of frames were counted the nucleation site count would slowly creep up as spurious points were counted. There are several potential forms of error in this methodology. The first is from the choice of the

heuristics for selecting a site. These include the signal cutoff value, the convergence criteria, and the maximum site size. These were varied to explore the sensitivity, and within the reasonable range of possible choices affected the outcome by about 6% and this is the value represented by the error bars in Figure 5. The cutoff value has to be restrictive enough to be able to distinguish at low heat fluxes between nucleation events and the thermal effects of a sliding bubble, but not so restrictive that sites are missed. There is also the error associated with camera spatial resolution. The spatial resolution of the pixels are 90  $\mu\text{m}$  and as the site density gets higher there will be more missed sites because of the increased likelihood of sites overlapping that are closer together than the resolution of the camera. The automatic MATLAB-based counting algorithm was validated by comparing it to manual counting and found to agree within 10%. However, the automatic site counter was consistently larger, and would identify sites missed during the hand counting.

The nucleation site model proposed by Kocamustafaogullari and Ishii [31, 32] is shown in (1)-(4) and shown along with the plot for a mass flux of 1250  $\text{kg}/\text{m}^2/\text{s}$ . This model was chosen as a reference because it is applicable to flow boiling, and the parameters that make up the model are readily deduced from the experimental data. The departure diameter was taken from the experimental data rather than using a model to estimate it.

$$N_{np}^* = f(\rho^*) R_c^{*-4.4} \quad N_{np}^* = N_{np} D_d^2 \quad (1)$$

$$f(\rho^*) = 2.157 \times 10^{-7} \rho^{*-3.2} (1 + 0.0049 \rho^*)^{4.13} \quad \rho^* = (\rho_f - \rho_g) / \rho_g \quad (2)$$

$$R_c^* = R_c / (D_d / 2) \quad R_c = \frac{2\sigma \{1 + \rho_f / \rho_g\} / P_f}{\exp\{i_{fg} (\Delta T_e) / (RT_g T_{sat})\} - 1} \quad \Delta T_e = S(T_g - T_{sat}) \quad (3)$$

$$S = (1 + 1.5 \times 10^{-5} \text{Re}_{TP})^{-1} \quad \text{Re}_{TP} = (G(1-x)D / \mu_f) F^{1.25} \quad (4)$$

$N_{np}$  is the nucleation site density ( $\text{m}^{-2}$ ),  $R_c$  is the effective critical cavity size (m),  $\rho_g$  is the density of the vapor ( $\text{kg}/\text{m}^3$ ),  $\rho_f$  is the density of the liquid ( $\text{kg}/\text{m}^3$ ),  $D_d$  is the departure diameter (m),  $\sigma$  is the surface tension (N/m),  $P_f$  is the liquid pressure ( $\text{N}/\text{m}^2$ ),  $i_{fg}$  is the heat of vaporization (J/kg),  $R$  is the gas constant (J/kg/K),  $\Delta T_e$  is the effective wall superheat (K),  $T_g$  is the vapor temperature (K),  $T_{sat}$  is the saturation temperature (K),  $G$  is the mass flux ( $\text{kg}/\text{m}^2/\text{s}$ ),  $x$  is the quality,  $D$  is the hydraulic diameter (m),  $\mu_f$  is the viscosity of the fluid,  $F=1$  for cases where the Martinelli parameter is  $> 10$ .

The measured values of the nucleation site density for a given wall superheat are lower than predicted by the model. This is likely because the model does not explicitly deal with subcooling of the bulk fluid. Instead the model is extended from a pool boiling model, and uses a correction factor to  $S$  to calculate the effective wall superheat from the actual wall superheat to account for the convective heat transfer mechanisms. Also, it is important to recognize that nucleation site density depends on the number of microcavities present on a surface, a dependence that is not considered by the Kocamustafaogullari and Ishii model.

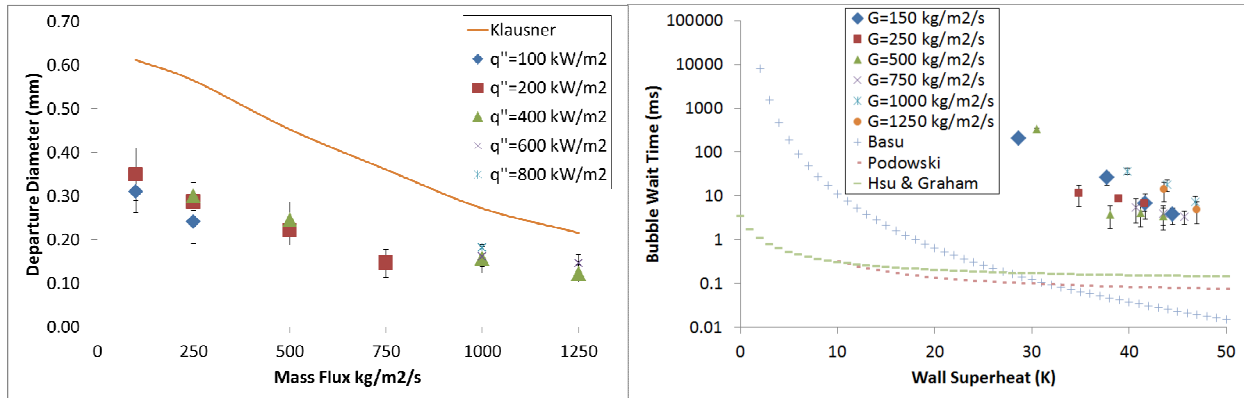


Figure 4 - Bubble departure diameters (left) and bubble wait times (right).

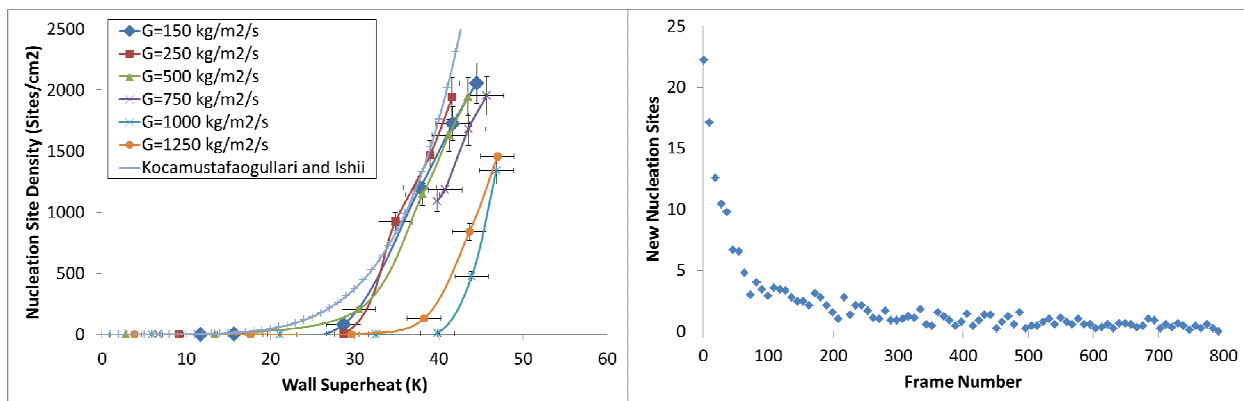


Figure 5 - Nucleation site density vs. wall superheat (left), and site counting convergence plot (right).

### 3.3 Temperature Profile of a Single Sliding Bubble

In addition to the ensemble data discussed in the previous section, the experiment can also be used to capture more detailed data on individual bubbles. An example is shown in Figure 6 for a low heat flux of 130 kW/m<sup>2</sup>/s, a mass flux of 200 kg/m<sup>2</sup>/s, and 10°C subcooling. A single bubble was examined as it slid along the surface of the heater. The HSV images were taken from the front. Both images are scaled the same to the bar shown in the HSV images.

The temperature profile along the path of the sliding bubble is shown in Figure 7. The small increase in the temperature along the heater surface in the direction of the flow is due to single-phase convective heat transfer to the fluid. As the bubble slides over the surface, the surface temperature drops, signaling significant localized cooling, which is likely due to evaporation of the liquid layer between the bubble and the wall. Approximately 80 ms after bubble passage, the surface temperature returns to the single-phase profile. Similar results were found for the individual bubbles observed in the study with similarly low heat fluxes and mass fluxes.

Whether a bubble departs from the wall by either sliding or detaching and entering the bulk fluid depends upon whether the force balance on the bubble is broken in the direction of the flow or perpendicular to the flow first [2, 17]. At low mass fluxes drag force and buoyancy dominate thus tending to make the bubble slide along the surface. At higher mass fluxes shear lift forces begin to become more dominant and make the bubble tend to depart normal to the flow. This is

consistent with observations of Dix [33] and Saha and Zuber [34] that observed at lower Peclet numbers ( $< 70,000$ ) bubbles tend to slide while at higher Peclet numbers the bubbles tend to detach from the wall.

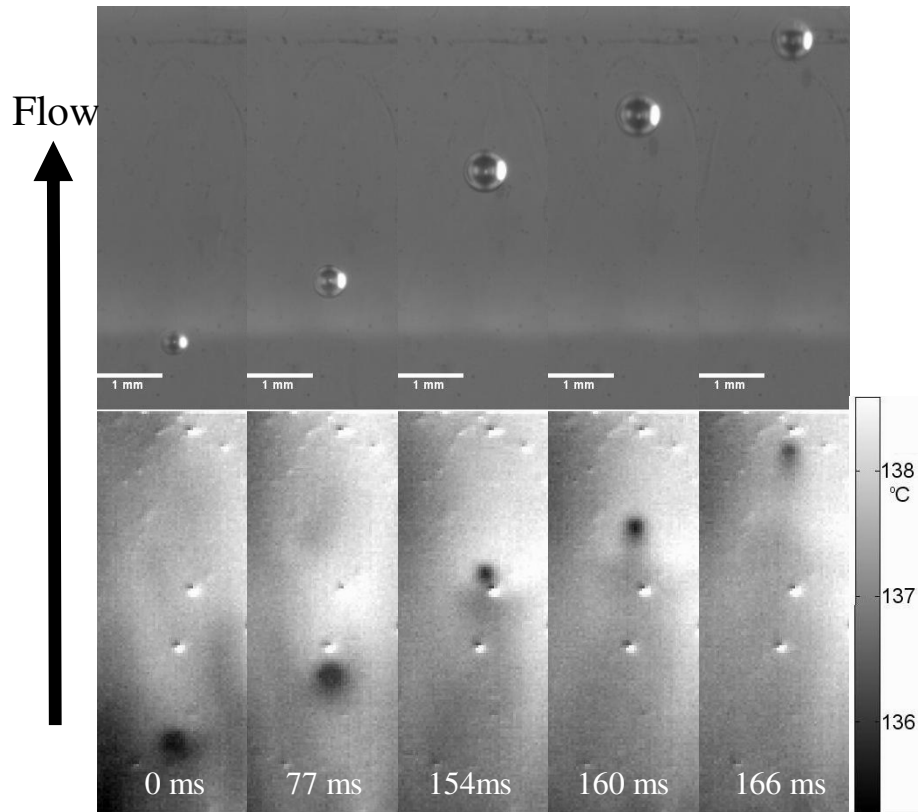


Figure 6 - HSV (top) and IR (bottom) of a bubble from the onset of sliding ( $t=0$  ms) to the end of the frame ( $t=166$  ms).

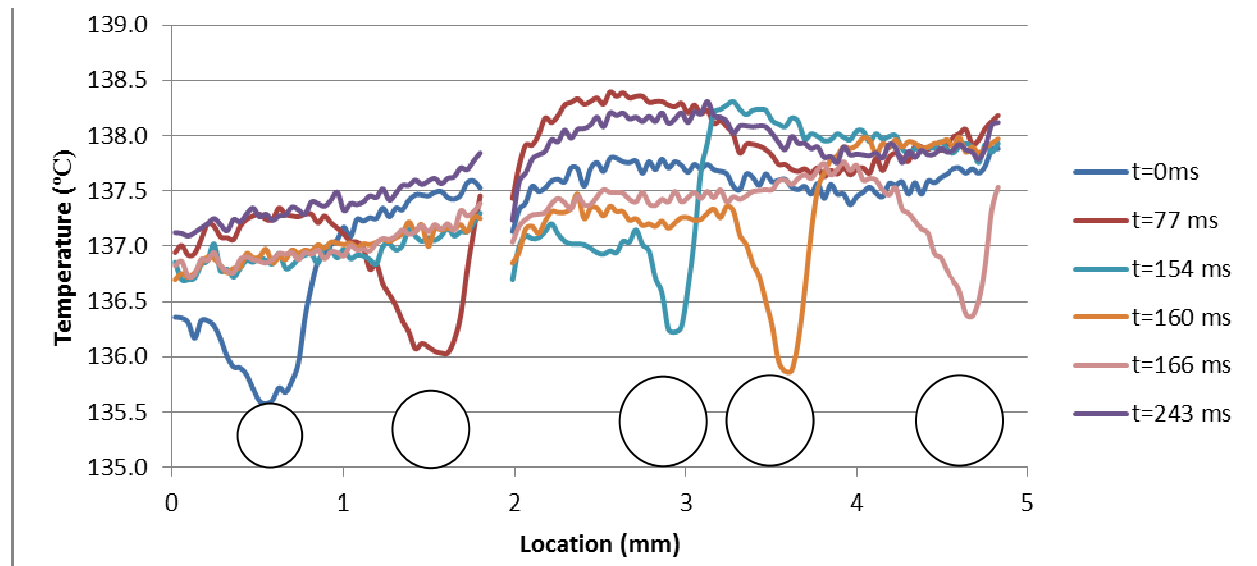


Figure 7 - Temperature profile along the sliding bubble path at various time steps.  $t=0$  is the onset of bubble sliding. The circles on the plot show the approximate position of the bubble at each time step. (The measurement uncertainty on temperature is  $\pm 2.0^\circ\text{C}$ ; error bars not shown)

The cooling underneath a bubble as it slides was measured for various conditions. This heat transfer mechanism is one that is ignored in mechanistic models. The temperature was measured via IR thermography and was plotted for constant nucleation site density. An average of approximately 20 sliding bubbles was used for each point. To be considered the bubble had to nucleate on the surface, slide a minimum of 0.5 mm, and not be influenced by another bubble. The sliding velocity was also measured for the same set of bubbles and both are shown below in Figure 8.

There does not seem to be a clear trend for the cooling under a sliding bubble as a function of mass flux. The value is rather constant and varies roughly between 2-4°C. The velocity of a sliding bubble increases almost linearly with mass flux. There seems to be no strong dependence on the heat flux. At low mass fluxes the bubbles move at nearly the same speed as the bulk flow and at higher mass fluxes the bubbles move at 50-60% of the speed of the bulk flow. However, the bubbles are near the wall where the velocity is less than that of the bulk fluid.

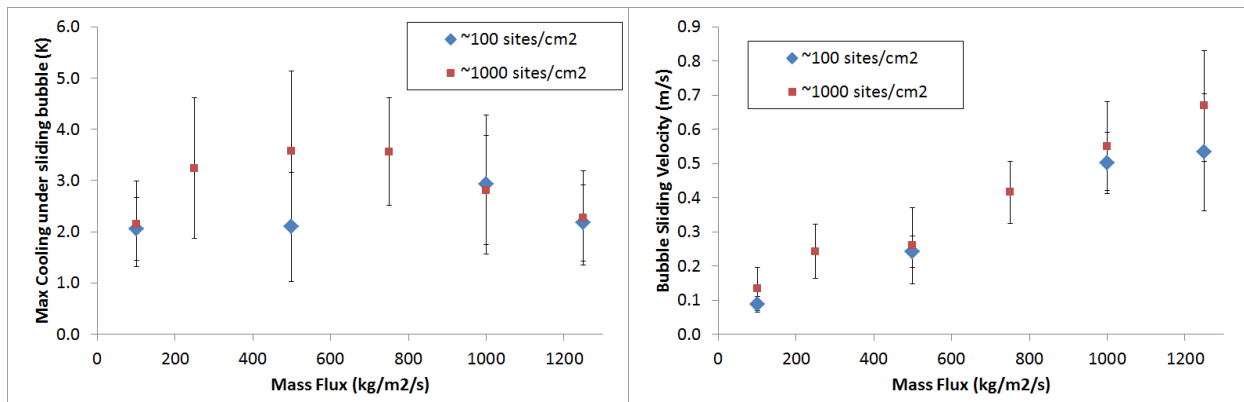


Figure 8 – Maximum cooling under a sliding bubble vs. mass flux (left) and velocity of sliding bubbles vs. mass flux (right).

### 3.4 Temperature Profile vs. Time for High Heat Flux

An example with a higher heat flux of 600 kW/m<sup>2</sup>-s, a mass flux of 200 kg/m<sup>2</sup>-s, and 9°C subcooling is shown in Figure 8. The temperature history of the nucleation site circled in red is shown in Figure 9, this shows the temperature of the center of the nucleation site as a function of time. Four complete ebullition cycles are shown. The time during which the temperature rises represents the wait time, while the surface is heating up after the previous bubble formation. Then the bubble nucleates, grows and departs, which determines the fast drop in temperature, and the cycle repeats.

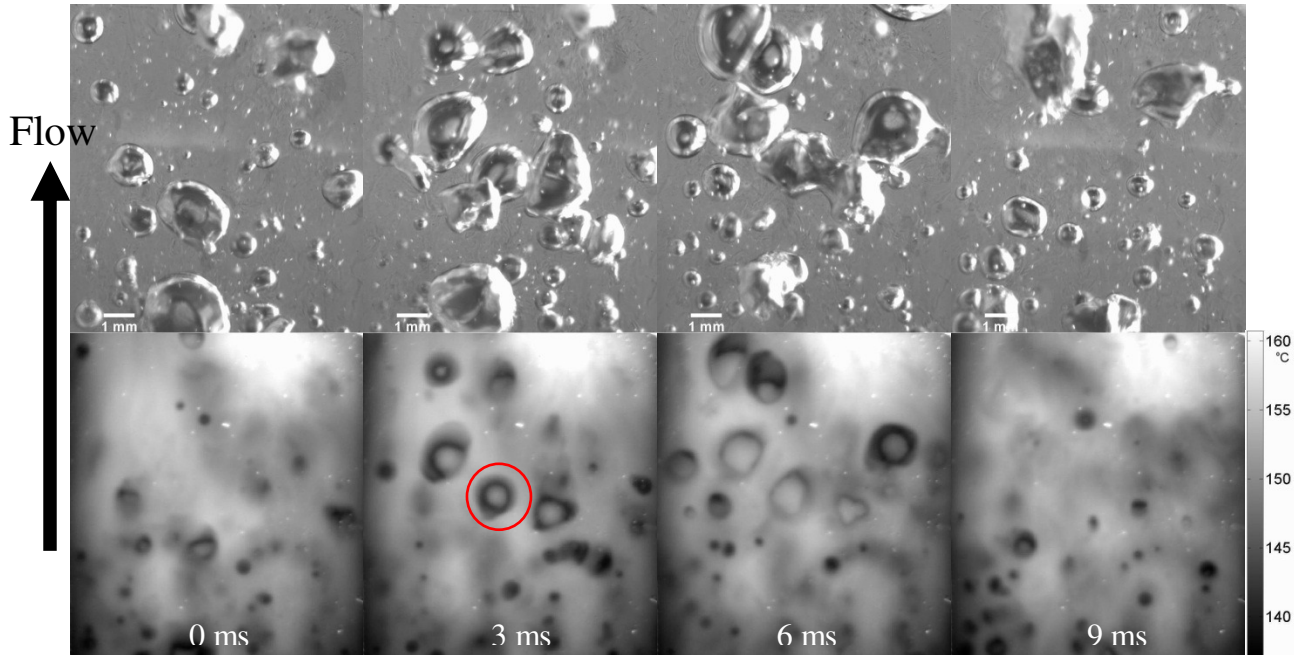


Figure 9 – HSV (top) and IR (bottom) images for a high heat flux case.

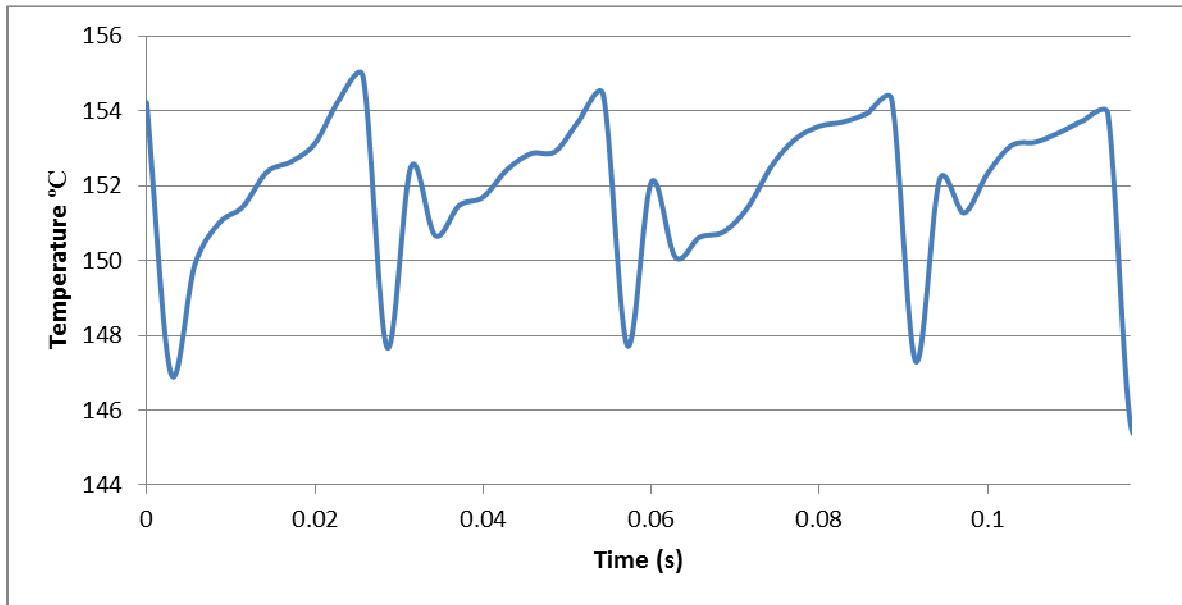


Figure 10 – Average surface temperature vs. time for 0.1 mm radius on heater surface at nucleation site circled in red in Figure 9.

#### 4. CONCLUSIONS

Several key subcooled flow boiling quantities were successfully measured simultaneously including bubble departure diameter, bubble wait time, bubble sliding velocity, cooling under sliding bubbles, nucleation site density, the wall superheat, and heat transfer coefficient, using High-Speed Video (HSV) and IR thermography.

Existing models for nucleation site density and bubble wait time do not accurately capture the data, because they do not account for important effects such as fluid subcooling and heater thermal diffusivity, i.e. nucleation site density is expected to decrease with increasing subcooling; wait time is expected to increase with increasing subcooling and decreasing heater thermal diffusivity.

Synchronized IR and HSV images of individual bubbles sliding along the wall revealed that significant localized cooling occurs at the wall underneath a sliding bubble, likely from evaporation of the liquid film sandwiched between the bubble and the wall. The cooling does not appear to have a strong dependence on heat flux or mass flux. This cooling effect should be accounted for in future mechanistic models of subcooled flow boiling heat transfer.

## 5. ACKNOWLEDGEMENTS

The Consortium for Advanced Simulation of Light Water Reactors (CASL) and National Science Foundation Graduate Research Fellowship Program (NSFGRFP) are gratefully acknowledged for their support of this work. Additional thanks to Eric Forrest for his valuable help in the lab, and to Rosie Sugrue for sharing her work on bubble departure diameters.

## 6. REFERENCES

- [1] M. Ishii and T. Hibiki, *Thermo-Fluid Dynamics of Two-Phase Flow*. Springer, 2011.
- [2] N. Kurul and M. Podowski, "Multidimensional effects in forced convection subcooled boiling," in *Proceedings of the Ninth International Heat Transfer Conference*, Jerusalem, Israel, 1990.
- [3] N. Kolev, "How accurately can we predict nucleate boiling?" in *Multiphase Flow Dynamics 3*. Springer Berlin Heidelberg, 2012, pp. 143–178.
- [4] V. H. D. Valle and D. Kenning, "Subcooled flow boiling at high heat flux," *International Journal of Heat and Mass Transfer*, vol. 28, no. 10, pp. 1907–1920, 1985.
- [5] N. Basu, G. R. Warrier, and V. K. Dhir, "Onset of nucleate boiling and active nucleation site density during subcooled flow boiling," *Journal of Heat Transfer*, vol. 124, pp. 717–728, 2002.
- [6] R. Situ, Y. Mi, M. Ishii, and M. Mori, "Photographic study of bubble behaviors in forced convection subcooled boiling," *International Journal of Heat and Mass Transfer*, vol. 47, no. 17-18, pp. 3659–3667, 2004.
- [7] R. Situ, M. Ishii, T. Hibiki, J. Tu, G. Yeoh, and M. Mori, "Bubble departure frequency in forced convective subcooled boiling flow," *International Journal of Heat and Mass Transfer*, vol. 51, no. 25-26, pp. 6268–6282, 2008.
- [8] G. Hong, X. Yan, Y. hua Yang, T. zhou Xie, and J. jun Xu, "Bubble departure size in forced convective subcooled boiling flow under static and heaving conditions," *Nuclear Engineering and Design*, vol. 247, no. 0, pp. 202–211, 2012.
- [9] D. Euh, B. Ozar, T. Hibiki, M. Ishii, and C.-H. Song, "Characteristics of bubble departure frequency in a low-pressure subcooled boiling flow," *Journal of Nuclear Science and Technology*, vol. 47, no. 7, pp. 608–617, 2010.

- [10] N. Basu, G. R. Warriar, and V. K. Dhir, "Wall heat flux partitioning during subcooled flow boiling: Part 1-model development," *Journal of Heat Transfer*, vol. 127, pp. 131–140, February 2005.
- [11] R. M. Podowski, D. A. Drew, R. T. L. Jr., and M. Z. Podowski, "A mechanistic model of the ebullition cycle in forced-convection subcooled boiling," in *Proceedings of the 8th International Topical Meeting on Nuclear Reactor Thermal Hydraulics (NURETH-8)*, vol. 3, Kyoto, Japan, September-October 1997, pp. 1530–1537.
- [12] G. Thorncroft, J. Klausner, and R. Mei, "An experimental investigation of bubble growth and detachment in vertical upflow and downflow boiling," *International Journal of Heat and Mass Transfer*, vol. 41, no. 23, pp. 3857–3871, 1998.
- [13] R. Ahmadi, T. Ueno, and T. Okawa, "Bubble dynamics at boiling incipience in subcooled upward flow boiling," *International Journal of Heat and Mass Transfer*, vol. 55, no. 1-3, pp. 488–497, 2012.
- [14] S. Li, S. Tan, C. Xu, P. Gao, and L. Sun, "An experimental study of bubble sliding characteristics in narrow channel," *International Journal of Heat and Mass Transfer*, vol. 57, no. 1, pp. 89–99, 2013.
- [15] C. Hutter, K. Sefiane, T. Karayiannis, A. Walton, R. Nelson, and D. Kenning, "Nucleation site interaction between artificial cavities during nucleate pool boiling on silicon with integrated micro-heater and temperature micro-sensors," *International Journal of Heat and Mass Transfer*, vol. 55, no. 11-12, pp. 2769 – 2778, 2012.
- [16] C. Chen, W. Chang, K. Li, Y. Lie, and T. Lin, "Subcooled flow boiling heat transfer of r-407c and associated bubble characteristics in a narrow annular duct," *International Journal of Heat and Mass Transfer*, vol. 52, no. 13-14, pp. 3147–3158, 2009.
- [17] R. Sugrue, T. McKrell, and J. Buongiorno, "On the effects of orientation angle, subcooling, mass flux, heat flux, and pressure on bubble departure diameter in subcooled flow boiling," in *Proceedings of Computational Fluid Dynamics in Nuclear Reactor Safety - 4*, 2012.
- [18] C. D. Gerardi, "Investigation of the pool boiling heat transfer enhancement of nano-engineered fluids by means of high-speed infrared thermography," Ph.D. dissertation, Massachusetts Institute of Technology, May 2009.
- [19] T. Theofanous, J. Tu, A. Dinh, and T. Dinh, "The boiling crisis phenomenon: Part I: nucleation and nucleate boiling heat transfer," *Experimental Thermal and Fluid Science*, vol. 26, no. 6-7, pp. 775–792, 2002.
- [20] T. Theofanous, T. Dinh, J. Tu, and A. Dinh, "The boiling crisis phenomenon: Part II: dryout dynamics and burnout," *Experimental Thermal and Fluid Science*, vol. 26, no. 6-7, pp. 793–810, 2002.
- [21] E. Wagner and P. Stephan, "High-resolution measurements at nucleate boiling of pure FC-84 and FC-3284 and its binary mixtures," *Journal of Heat Transfer*, vol. 131, pp. 121008–1, 2009.
- [22] C. Gerardi, J. Buongiorno, L.-w. Hu, and T. McKrell, "Infrared thermometry study of nanofluid pool boiling phenomena," *Nanoscale Research Letters*, vol. 6, no. 1, p. 232, 2011.

- [23] C. Gerardi, J. Buongiorno, L. wen Hu, and T. McKrell, "Study of bubble growth in water pool boiling through synchronized, infrared thermometry and high-speed video," *International Journal of Heat and Mass Transfer*, vol. 53, no. 19, pp. 4185–4192, 2010.
- [24] I. Golobic, J. Petkovsek, and D. Kenning, "Bubble growth and horizontal coalescence in saturated pool boiling on a titanium foil, investigated by high-speed ir thermography," *International Journal of Heat and Mass Transfer*, vol. 55, no. 4, pp. 1385–1402, 2012.
- [25] M. C. Díaz, H. Boye, I. Hapke, J. Schmidt, Y. Staate, and Z. Zhekov, "Investigation of flow boiling in narrow channels by thermographic measurement of local wall temperatures," *Microfluidics and Nanofluidics*, vol. 2, pp. 1–11, 2005.
- [26] G. L. DeWitt, "Investigation of downward facing critical heat flux with water-based nanofluids for in-vessel retention applications," Ph.D. dissertation, Massachusetts Institute of Technology, September 2011.
- [27] J. G. Collier and J. R. Thome, *Convective Boiling and Condensation*, 3rd ed. Oxford University Press, 1994.
- [28] J. Klausner, R. Mei, D. Bernhard, and L. Zeng, "Vapor bubble departure in forced convection boiling," *International Journal of Heat and Mass Transfer*, vol. 36, no. 3, pp. 651–662, 1993.
- [29] M. Z. Podowski and R. M. Podowski, "Mechanistic multidimensional modeling of forced convection boiling heat transfer," *Science and Technology of Nuclear Installations*, vol. 2009, p. 387020, 2009.
- [30] Y.-Y. Hsu and R. W. Graham, *Transport Processes in boiling and Two-Phase Systems*. American Nuclear Society, 1986.
- [31] G. Kocamustafaogullari and M. Ishii, "Interfacial area and nucleation site density in boiling systems," *International Journal of Heat and Mass Transfer*, vol. 26, no. 9, pp. 1377 – 1387, 1983.
- [32] T. Hibiki and M. Ishii, "Active nucleation site density in boiling systems," *International Journal of Heat and Mass Transfer*, vol. 46, no. 14, pp. 2587 – 2601, 2003.
- [33] G. E. Dix, "Vapor void fractions for forced convection with subcooled boiling at low flow rates." Ph.D. dissertation, University of California, Berkley, December 1971.
- [34] P. Saha and N. Zuber, "Point of net vapor generation and vapor void fraction in subcooled boiling," in *Proceedings of the 5th International Heat Transfer Conference, Tokyo*, vol. 4, 1974, pp. 175–179.